ADVANCING EARTH AND SPACE SCIENCES

Geophysical Research Letters

RESEARCH LETTER
10.1029/2025GL117468

Turbulent Mixing in the Upper Arctic Ocean Energized by Interactions of Tidally-Forced Waves With Mesoscale Shear

S. F. Reifenberg[1] and **I. Fer**[2]

[1]Alfred Wegener Institute for Polar and Marine Research, Bremerhaven, Germany, [2]Geophysical Institute, University of Bergen, and Bjerknes Center for Climate Research, Bergen, Norway

Key Points:

- High-resolution observations of a warm-core eddy in ice-covered northern Fram Strait revealed complex interactions across scales
- Upward-propagating tidally-generated internal waves enhance mixing in the meltwater halocline
- Mesoscale variability modulates the internal wave shear and thus influences energy transfers and ecosystem dynamics in the upper ocean

Supporting Information:

Supporting Information may be found in the online version of this article.

Correspondence to:

S. F. Reifenberg,
simon.reifenberg@awi.de

Citation:

Reifenberg, S. F., & Fer, I. (2025). Turbulent mixing in the upper Arctic Ocean energized by interactions of tidally-forced waves with mesoscale shear. *Geophysical Research Letters*, *52*, e2025GL117468. https://doi.org/10.1029/2025GL117468

Received 6 JUN 2025
Accepted 24 JUN 2025

Abstract

High-resolution observations in Fram Strait reveal complex interactions across scales, highlighting the role of internal waves in enhancing mixing within the meltwater halocline. A day-long microstructure survey from drifting ice that traversed an anticyclone in summer shows rotating shear and straining in the halocline, resulting in low Richardson number layers coincident with turbulent patches and gradients in oxygen and chlorophyll. Year-long data from an adjacent mooring demonstrate that increased shear variance can be related to upward-propagating wave energy, generated by tidal forcing at the seafloor and amplified by mesoscale shear near the surface. These waves contain compound tides and overtones with spectral peaks at 3 and 4 cycles per day. Mesoscale variability modulates internal wave shear, influencing turbulent mixing and ecosystem dynamics. Our findings underscore the importance of cross-scale interactions in driving turbulent mixing, with implications for water mass transformations, sea ice melt, and primary production in a changing Arctic.

Plain Language Summary

Warm Atlantic waters flow into the Arctic Ocean and contribute to sea ice loss, affecting the global ocean circulation and climate. In Fram Strait, a deep passage between Svalbard and Greenland, heavier Atlantic-origin waters dive beneath Arctic-origin waters. Consequently, observing the mixing processes bringing this subsurface heat up to the ice-covered surface is important for understanding the ongoing changes in the Arctic. Here, we analyze measurements in the water column from a drifting ice station (one day long) and instruments from a bottom-anchored line (1 year long) to investigate these mixing mechanisms. We show that large swirling currents (about >6 km diameter) interact with small velocity fluctuations produced by tidal currents at the seafloor. The interaction amplifies the effect of the small fluctuations on mixing in the upper ocean. Ice melt in summer accumulates a layer of light water in upper ocean, which becomes difficult to mix vertically (like oil on water). As turbulence energy is required to move heat or nutrients from deeper layers to the surface, the suggested interaction offers an additional source of energy for mixing in the surface layer, and is relevant for sea ice and the ecosystem.

1. Introduction

In the Arctic Ocean, the inflow of warm Atlantic Water (AW) plays an increasing role in sea ice loss and changes of the ecosystem (Ardyna & Arrigo, 2020; Carmack et al., 2015; Polyakov et al., 2025). Quantifying the processes contributing to vertical mixing of AW, and interactions between different scales of dynamical forcing, is critical to our understanding of the Arctic climate system (Rippeth & Fine, 2022).

Fram Strait (FS), between Svalbard and Greenland, is the only deep connection between the Atlantic and Arctic Oceans, where warm and haline AW is transported poleward by the West Spitsbergen Current (WSC, Figure 1a). This boundary current flows along the western slope of Svalbard, and splits into branches flowing around Svalbard, and across and around the Yermak Plateau (Artana et al., 2022; Athanase et al., 2021; Fer et al., 2023; Manley, 1995). In northern FS, the WSC subducts below the colder and fresher Polar Water, and partly recirculates southward, driven by eddies and modulated by atmospheric forcing (Hattermann et al., 2016; Hofmann et al., 2021; McPherson et al., 2023).

Fram Strait and particularly the Yermak Plateau region are characterized by strong tidal currents (Fer et al., 2015; Padman et al., 1992), energetic eddies (von Appen et al., 2016; Wekerle et al., 2020), southward advection of sea ice (Ivanov et al., 2016; Sumata et al., 2021), and a pronounced seasonal cycle (deep convective mixed layers in winter and shallow meltwater stratification during summer, e.g., Randelhoff et al. (2017); von Appen et al. (2021)). Here, the diurnal and most semidiurnal tides are subinertial and cannot generate freely propagating

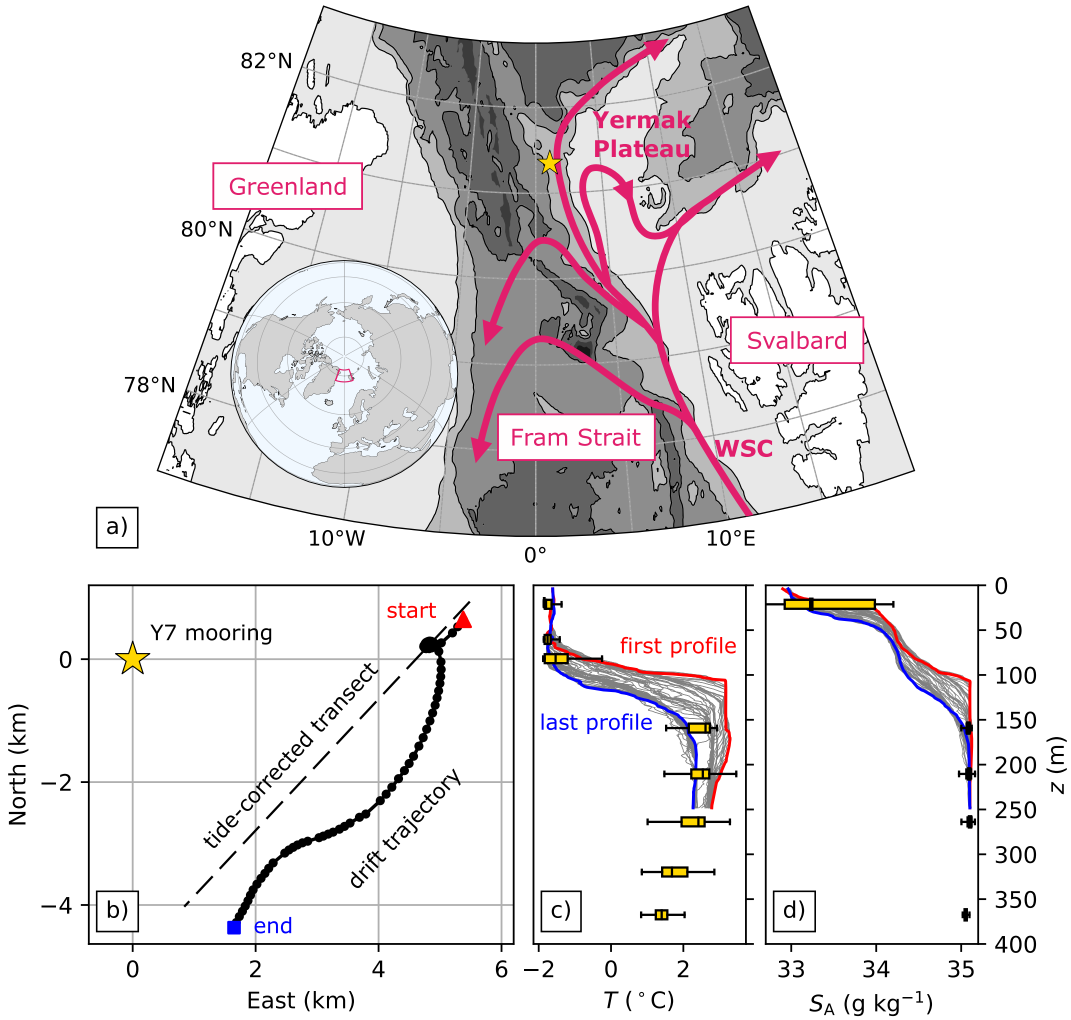

Figure 1. Sampling overview. (a) Map showing Fram Strait, Yermak Plateau, branches of the Atlantic Water inflow, the mooring location (yellow star), and isobaths every 1,000 m. (b) Close-up of the survey area, with mooring, drift trajectory (dots are profile positions), and the transect to which we remapped the drift observations (see Text S1 in Supporting Information S1). Vertical profiles of (c) in situ temperature T and (d) salinity S_{A}, from the MSS (gray: all profiles; red: first profile; blue: last profile), and from the year-long mooring observations (box-whisker plots at respective sensor depths).

linear internal tides, that is internal waves (IW) at the tidal forcing frequencies. However, the interaction of tides and topography can generate unsteady lee-waves (Fer et al., 2020; Reifenberg, Fer, et al., 2025; Rippeth et al., 2017), freely propagating overtones of diurnal tides (Baumann & Fer, 2023; Wang et al., 2022), or nonlinear solitary waves (Urbancic et al., 2022). Furthermore, as the inertial frequency is close to semidiurnal, a negative background relative vorticity, for instance from a mesoscale anticyclone or the horizontal shear of the boundary current (He & Lamb, 2022; Kunze, 1985), can reduce the effective inertial frequency, thereby allowing freely propagating semidiurnal internal tides.

The mean flow, mesoscale eddies, tides, and internal waves represent scale-separated energy compartments. Between these, kinetic energy is transferred through a range of processes, ultimately cascading down to small scales where it is dissipated. Sea ice modulates these transfers by altering atmosphere–ocean momentum fluxes (Martin et al., 2016), frictional under-ice dissipation (Manucharyan & Thompson, 2022), as well as surface stratification and potential energy (Manucharyan & Thompson, 2017). These dynamics also drive variability in marine ecosystems. For instance, the meltwater halocline limits vertical exchange, thereby suppressing nutrient fluxes into the euphotic zone (von Appen et al., 2021; Lester et al., 2021), and drives eukaryotic biodiversity and community composition under sea ice (Murray et al., 2025). The lateral transport of nutrients and heat by mesoscale processes, including eddies, can lead to localized phytoplankton blooms (Schourup-Kristensen et al., 2021).

Observing cross-scale energy transfers and subsequent mixing is challenging in the relatively inaccessible Arctic Ocean. Here, we present results from a sea ice-based microstructure survey, conducted during a day-long drift station that traversed the rim of a warm-core anticyclone. We describe its hydrographic structure and quantify key parameters for turbulent mixing. We observed upward-propagating internal waves driving mixing in the melt-water halocline, affecting a deep chlorophyll maximum, and discuss the eddy's role in altering the properties of these waves. Using year-long observations from an adjacent mooring, we place these results in a broader context.

2. Data and Methods

During the PS131 expedition with RV Polarstern in summer 2022, we made measurements from a drifting ice floe (27 July 22:15 UTC to 28 July 21:00 UTC).

Hydrographic variables and the rate of turbulent dissipation were obtained using a loosely-tethered microstructure profiler (MSS; Sea and Sun Technology, Germany). The MSS was deployed through a hole in the ice, sufficiently distanced from the wake of the ship. Within 22 hr, 68 profiles to 250 m depth were collected, with a median interval of 17 min between profiles. The MSS data and processing details are available from Fer and Reifenberg (2025a). Dissipation estimates from shear probes followed best practices recommendations from Lueck et al. (2024), and we tested our routines successfully against benchmark data sets (Fer et al., 2024). The lowest dissipation rates, that is the lower detection limit, is $\sim 10^{-9}$ W kg^{-1}. Ocean current velocities were observed from an ice-mounted Acoustic Doppler Current Profiler (ADCP; 300 kHz, 2-m vertical resolution down to $\sim$80-m depth; Teledyne RDI, USA) and the vessel-mounted ADCP (150 kHz, 4-m cells down to 250 m; Teledyne RDI, USA). We project the observations from the drift trajectory onto a target transect (Figure 1b) by removing the tidal influence as described in Text S1 in Supporting Information S1.

We calculate the Conservative Temperature, Θ, Absolute Salinity, S_{A}, potential density anomaly, σ_0, and the buoyancy frequency, N, using TEOS-10 (McDougall & Barker, 2011), and apparent oxygen utilization (AOU) as the difference from saturation concentration and observed concentration of dissolved oxygen: AOU $= [\mathrm{O_2}]_{\mathrm{sat}} - [\mathrm{O_2}]_{\mathrm{obs}}$. We subtract a constant offset of 67.5 μmol kg^{-1} from $[\mathrm{O_2}]_{\mathrm{obs}}$, based on a comparison with measurements from the ship's CTD system, which were calibrated against water samples.

A mooring ("Y7"; 81.3495°N, 1.0723°E, 1,535 m depth) was deployed 3 hr before, and 5 km to the west of the start of the drift station. It was recovered on 28 June 2023. The instrumentation is detailed in Table S1 in Supporting Information S1. The study site is on the western slope of the Yermak Plateau, north of the known northern AW recirculation (Hofmann et al., 2021) and the bifurcation of the Yermak Pass Branch (Artana et al., 2022), and was permanently ice-covered throughout the deployment period (Figure S1 in Supporting Information S1). The data and processing details are available from Fer et al. (2025). Temperature and salinity records are corrected using a calibration cast with instruments attached to the shipboard profiling system. Records from all instruments are hourly bin-averaged and interpolated to a common time array, corrected for mooring blow-downs, and vertically interpolated to 5-m resolution.

We describe the anticyclone seen in the MSS survey, which is also captured in the mooring data, using the moored observations, as detailed in Text S2 in Supporting Information S1. By fitting a Rankine vortex to the moored velocity field, we estimate the radius ($L = 6.5$ km) and maximum azimuthal velocity ($v_a = 0.17$ m s^{-1}) of an idealized eddy, yielding a Rossby number of Ro $= \frac{v_a}{Lf} \approx 0.2$.

From the mooring data, we estimate the mesoscale currents $\mathbf{u}_{\mathrm{meso}} = (u_{\mathrm{meso}}, v_{\mathrm{meso}})$ using bandpassed velocities between 35 hr and 15 days, and the shear in mesoscales as $\mathbf{S}_{\mathrm{meso}} = \partial \mathbf{u}_{\mathrm{meso}}/\partial z$. We approximate baroclinic velocity fluctuations by removing the depth-averaged velocity, $\mathbf{u}'(t,z) = \mathbf{u}(t,z) - \mathbf{u}_0(t)$. We decompose $\mathbf{u}'$ into contributions of upward ($\mathbf{u}'_\uparrow$) and downward ($\mathbf{u}'_\downarrow$) propagating internal wave energy using two-dimensional fft-filtering on frequency-vertical wavenumber space, following Fer (2014); Voet et al. (2024). We quantify the energy and shear of upward-propagating waves using $\mathbf{u}'_\uparrow = (u'_\uparrow, v'_\uparrow)$ bandpassed between 1.7 and 4.3 cpd (cycles per day). This band contains near-inertial waves and first tidal overtones. The horizontal kinetic energy and shear associated with upward-propagating IW are then $\mathrm{HKE}_\uparrow = 1/2\left[(u'_\uparrow)^2 + (v'_\uparrow)^2\right]$ and $\mathbf{S}_\uparrow = \partial \mathbf{u}'_\uparrow/\partial z$, respectively.

The spectral variance of $\mathbf{u}'(t, z)$ is estimated by half-overlapping ~85-day long windows, which allows sufficient frequency resolution to separate diurnal (ω_{K_1}, ω_{O_1}), semidiurnal (ω_{M_2}, ω_{S_2}) tidal frequencies. For the microstructure survey, shear is decomposed into oscillating components by harmonic regression (informed by mooring spectra, see Results).

The Richardson number $\mathrm{Ri} = N^2/S^2$ (where S^2 is velocity shear magnitude), a measure for dynamical stability, is calculated using 4-m gradients. The Ozmidov length scale $L_\mathrm{O} = \left(\varepsilon/N^3\right)^{1/2}$, the length scale of the largest turbulent eddies in a stratified fluid, is typically less than 1 m in our observations.

Information about the atmospheric background state and ice cover are based on ERA5 reanalysis (Hersbach et al., 2023).

3. Results

We first present results from the microstructure survey. An inspection of drivers for halocline mixing reveals a potential link between wave-driven mixing and the presence of the eddy. We then use the mooring data to support a generalized hypothesis of the relation between near-surface mixing and mesoscale activity.

3.1. Hydrographic Structure During the Survey

The water column sampled during the drift of the ice station can be characterized by a salinity-stratified layer extending to $z \approx 50$ m depth (or $\sigma_0 \approx 27.45$ kg m^{-3}) with temperatures close to freezing (the cold halocline layer, CHL), followed by a pronounced temperature gradient (the thermocline, between $\sigma_0 \approx 27.45 - 27.80$ kg m^{-3}), and a vertically uniform layer of relatively warm and haline water early in the record (Figures 1c and 1d; Figures 2a and 2b; Figure S2 in Supporting Information S1). There is no distinct surface mixed layer. The stratification is strongest in the CHL, with buoyancy frequency $N > 0.01$ rad s^{-1} (Figure 2c).

The warm, weakly-stratified layer at $x < 2$ km between 108 and 162 m is the core of an anticyclone captured in the first ~5 km of the transect (Figures 2b and 2c). The thickness of the weakly-stratified layer decreases toward the dynamic rim of the eddy at ~5 km, characterized by a subsurface velocity maximum (Figures 2d and 2e) and a sharp thermohaline front (Figure 2f), where the isotherms and isohalines are nearly perpendicular to the isopycnals.

The frontal region at the eddy rim exhibits a zig-zag pattern in Θ-S_A space (Figure S3 in Supporting Information S1), indicating steep thermohaline intrusions, with the ambient water being drawn downward at the front. This pattern is supported by the AOU signature, assuming it is a quasi-passive tracer (Figure 2h). Between 20 and 40 m depth and $x > 4$ km on the transect, there are distinct layers of enhanced chlorophyll-a concentration and oxygen supersaturation (AOU<0; Figures 2g and 2h). This is indicative of active or recent primary production, where phytoplankton converts nutrients and carbon dioxide into biomass while releasing oxygen.

More details on the finescale hydrography are provided in Text S3 in Supporting Information S1.

3.2. Internal Wave-Driven Mixing in the Cold Halocline

The observed dissipation rates span a range from the lowest detection limit to $\varepsilon \approx 1.5 \times 10^{-7}$ W kg^{-1}, generally decreasing with depth from the surface, but with intermittent patches of enhanced dissipation extending through the CHL (Figure 2i).

Dissipation near the thermohaline front is only slightly elevated (factor <2, Figure S3 in Supporting Information S1), and surface-forced turbulence is limited to the upper 20 m (Figure 3). The following detailed analysis of the velocity and dissipation measurements in the time domain in the upper 50 m shows that the turbulent patches in the CHL are driven by internal waves.

Surface-forced turbulence from wind-driven ice drift can be estimated from wind-to-ocean energy flux, typically proportional to the ice-relative current $|u_\mathrm{rel}|^3$ (e.g., Fer & Sundfjord, 2007, and references therein). In our observations, periods with elevated forcing (Figure 3a) coincide with shallow (<20 m) patches of enhanced dissipation (hatched areas in Figure 3), indicating that surface stress cannot explain the turbulence extending across the CHL.

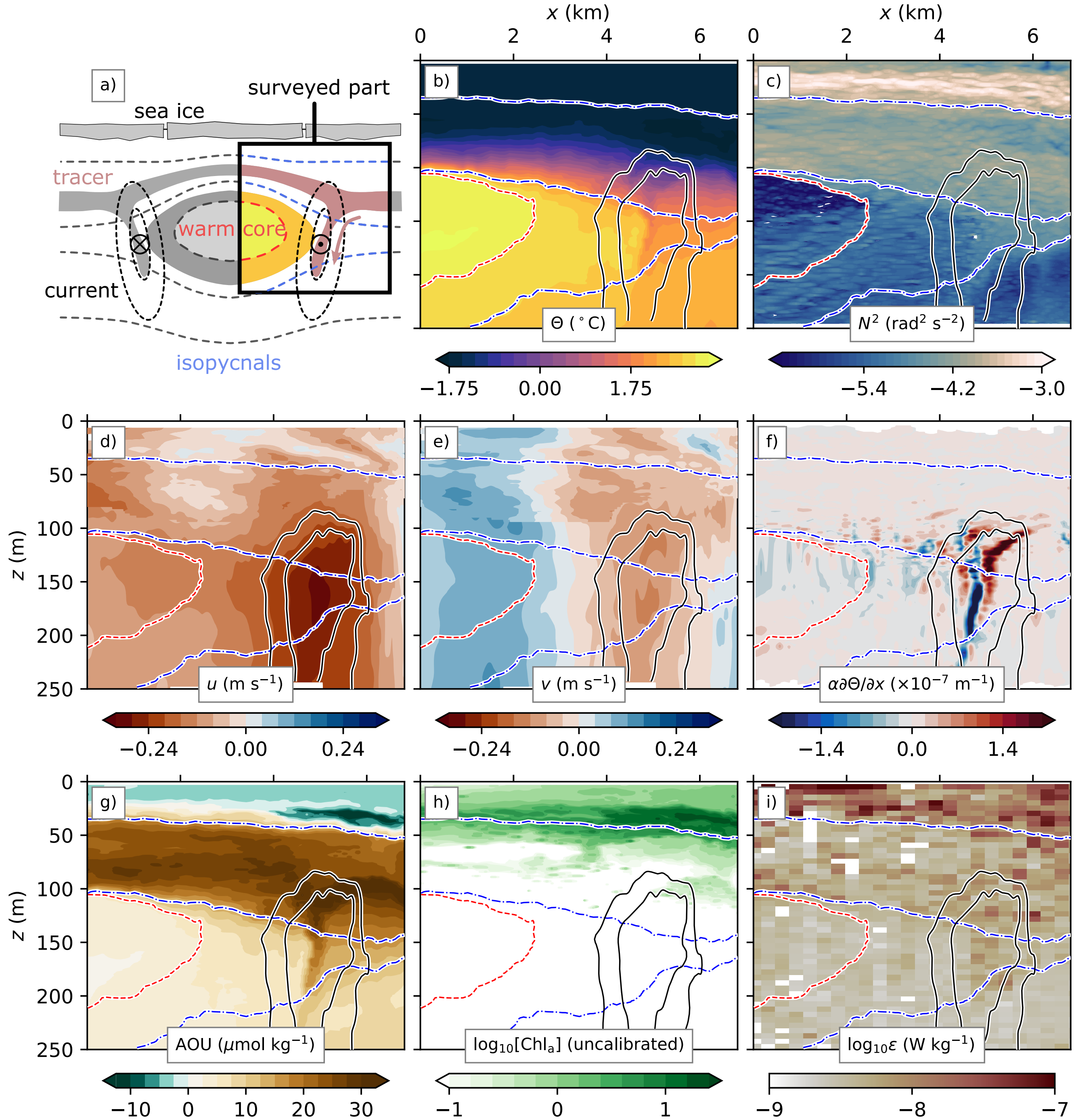

Figure 2. High-resolution survey of warm anticyclone. (a) Sketch based on the authors' interpretation of the observations. Depth-horizontal distance fields of (b) Conservative Temperature, (c) squared buoyancy frequency, (d) eastward and (e) northward horizontal velocity, (f) horizontal temperature gradient along isopycnals, (g) apparent oxygen utilization, (h) chlorophyll-a concentration, and (i) dissipation rate. In all panels, the 3°C isotherm (red dashed), 0.20 and 0.25 m s^{-1} isotachs (black solid), and 27.3, 27.8, 27.865 kg m^{-3} isopycnals (blue dashed) are indicated to facilitate comparisons.

In the stratified layer between 20 and 40 m, we observe coherent slanted layers of rotating velocity shear (Figures 3b and 3c). The shear bands coincide with vertical displacements of isopycnals and vertical velocity straining in the water column (Figures 3d and 3e). The gradient Richardson number attains low values, $\mathrm{Ri} \leq 1$ (Figure 3f), colocated with turbulent patches where $\varepsilon \geq 10^{-7.5}$ W kg^{-1}. These are strong indications for internal waves driving local turbulence through shear instability. The Ozmidov scale is $L_O < 1$ m in the halocline (not

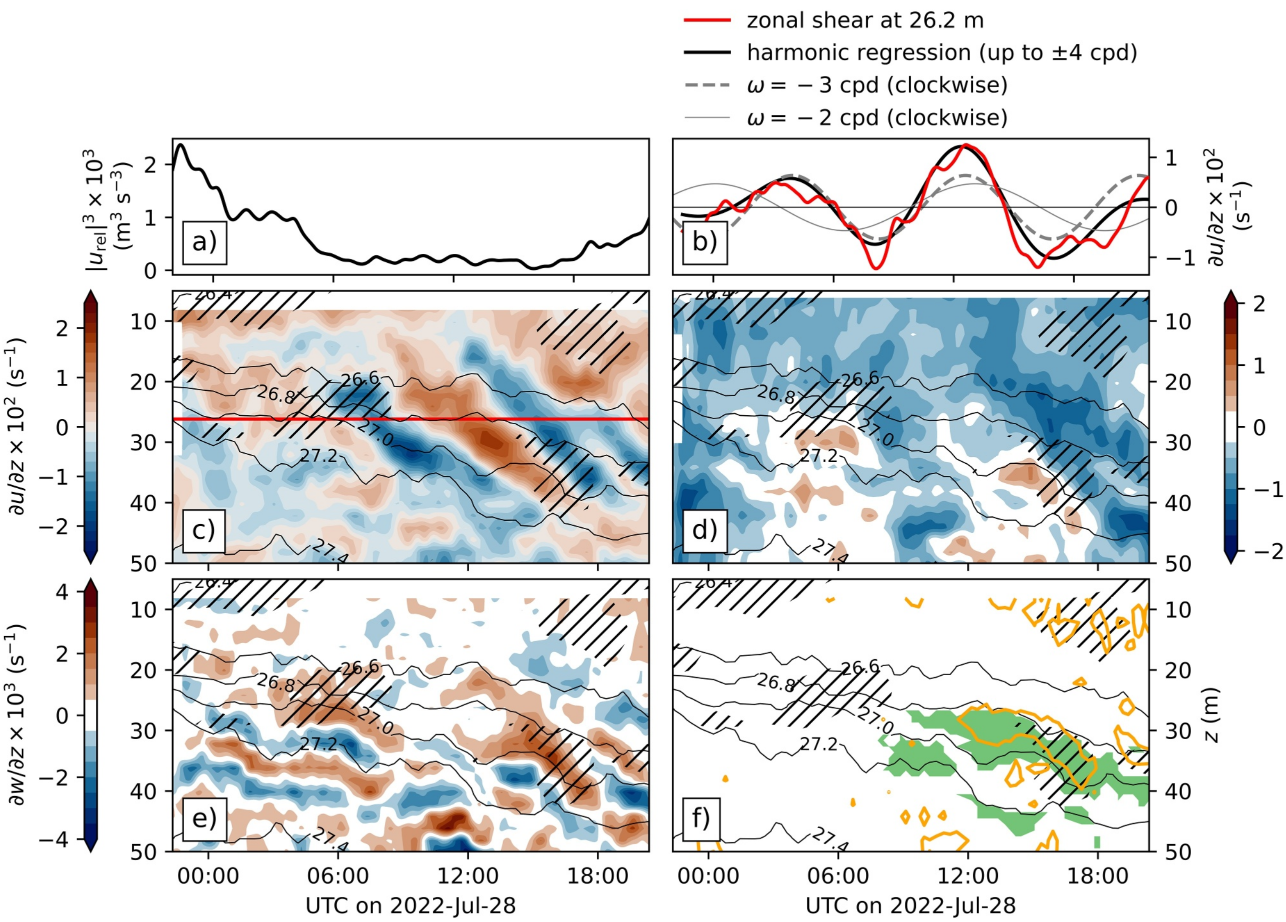

Figure 3. Internal wave signal in the upper ocean. (a) Cubed magnitude of the ice-relative ocean current u_{rel}, a proxy for the boundary forcing, (b) vertical shear of zonal current at example depth (26.2 m, red: observed; black and gray: from harmonic regression, see text), (c) zonal shear, red line marks the depth shown in (b, d) vertical velocity, (e) strain, (f) outline of the chlorophyll patch (green), orange lines outline patches with $\mathrm{Ri} \leq 1$. In (c–f), black contours are isopycnals and black hatching shows areas with $\varepsilon \geq 10^{-7.5}$ W kg^{-1}.

shown), hence our Ri estimate based on a coarser 4-m scale likely underestimates the shear from turbulent eddies (e.g., Silvester et al., 2014). Therefore, we consider $\mathrm{Ri} < 1$ a useful proxy for shear instability, and conclude that the internal waves drive the observed subsurface halocline turbulence. The turbulence patches coincide with sharp gradients in oxygen and chlorophyll-a, suggesting that this mixing pathway can be important in shaping the local biogeochemical cycles.

The observed waves are superinertial (here loosely defined as $1.2f < \omega \ll N$) and their energy propagates upward. The counterclockwise turning of the shear vector with depth indicates upward energy propagation (Leaman & Sanford, 1975). The time series is short for a detailed spectral analysis; however, from the interval between velocity extrema and the slope of the temporal evolution of wave phase, we estimate the frequency of the waves is in the range $\omega \approx 2.5$–3.5 cpd. We refine this estimate by a harmonic least-squares fit of superposed integer frequencies from −4 to 4 cpd, motivated by the mooring-based spectra (see below). The zonal shear from all fitted frequencies, and the clockwise 2-cpd and 3-cpd contributions, are compared to the observed shear in Figure 3b. The clockwise 3-cpd shear amplitude is the largest, followed by clockwise 2 cpd, showing a significant contribution from superinertial waves (local $f \approx 1.98$ cpd, $N > 100$ cpd).

3.3. Mooring-Based Evidence for Tidally-Forced Internal Waves

To investigate whether similar superinertial, upward-propagating waves are common in the region, we analyze the rotary spectra of $\mathbf{u}'$ and its decomposition into $\mathrm{HKE}_{\uparrow}$ and $\mathrm{HKE}_{\downarrow}$.

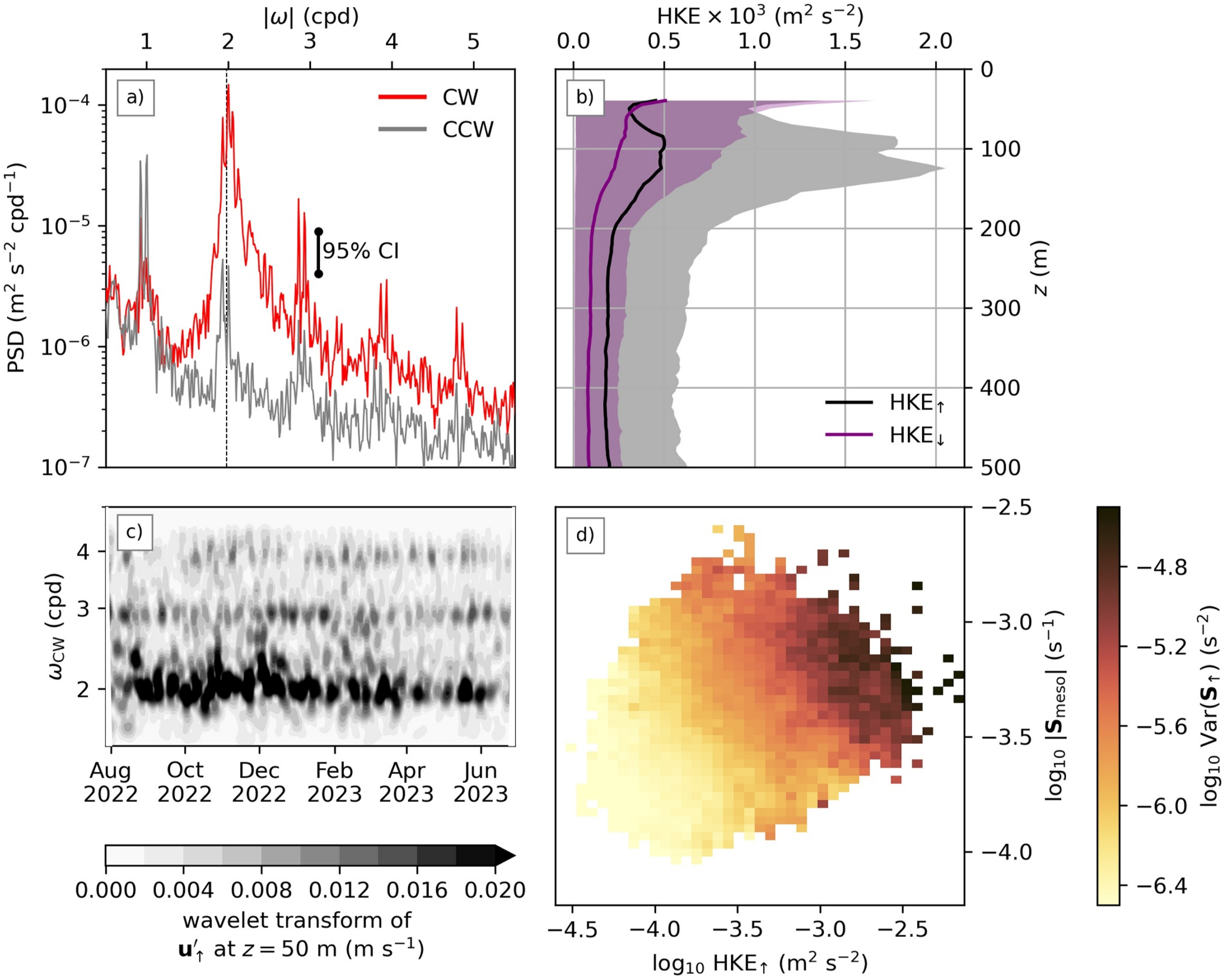

Figure 4. Mooring-based analysis. (a) Power spectral density (PSD) of $\mathbf{u}'$ at $z = 150$ m depth with 95% confidence interval (CI), showing clockwise (CW) and counterclockwise (CCW) contributions, and the inertial frequency (gray vertical line). (b) Profiles of horizontal kinetic energy associated with up- and downward energy propagation, shading indicates 5−95% percentiles. (c) Wavelet transform of $\mathbf{u}'_{\uparrow}$ at 50-m depth (clockwise frequencies). (d) Moving variance of $\mathbf{S}_{\uparrow}$, averaged into bins of internal wave horizontal kinetic energy $\mathrm{HKE}_{\uparrow}$ and shear of the background current in the eddy band $|\mathbf{S}_{\mathrm{meso}}|$. Only values above 300 m and bins with >25 samples are used.

In addition to a pronounced near-inertial peak, we find significant spectral peaks at approximately 3 and 4 cpd (clockwise), indicating that the local IW field is rather structured than purely stochastic (Figure 4a). These superinertial peaks, energized by nonlinear wave-wave interactions, are associated with tidal compound frequencies and overtones, for example $\omega_{\mathrm{O}_1} + \omega_{\mathrm{M}_2}$ and $2\omega_{\mathrm{M}_2}$ (Figure S4 in Supporting Information S1).

It is known that downward propagating energy, typically from wind-forced near-inertial waves, is a substantial driver of mixing in the Arctic Ocean (Fer, 2014); their impact is usually confined to the upper ocean. The velocity decomposition into $\mathbf{u}'_{\uparrow}$ and $\mathbf{u}'_{\downarrow}$ shows dominant energy associated with upward energy propagation, consistent with barotropic-to-baroclinic tidal conversion at the slope driving energy toward the surface (Figure 4b, Figure S5 in Supporting Information S1). The time-and-depth integrated $\mathrm{HKE}_{\uparrow}$ is larger than $\mathrm{HKE}_{\downarrow}$ by a factor of 1.6, suggesting an energy source at depth.

Given the tidal imprint on the IW spectrum, and the excess of upward-propagating energy, we suggest tidal forcing as the source of the ~3-cpd waves near the eddy, implying a link from tidal forcing over the seafloor to mixing in the surface layer.

3.4. Mesoscale Shear Amplifies Tidally-Forced Internal Waves

Background shear can significantly affect energy transfers and IW shear content. For example, Shakespeare and Hogg (2018) show that wave energy amplifies for waves propagating downward (vertical wavenumber $m < 0$) and with the shear flow ($k\partial u/\partial z > 0$, k is the horizontal wavenumber), and decays against the shear flow. The opposite behavior occurs for upward propagating waves. Provided that the internal waves in our microstructure survey propagate upward and offslope, they propagate with shear (energy decays) in the lower half and against shear (energy is amplified) in the upper half of the observed water column at 5 km (Figure 2d), consistent with our observations (Figure 3c). Thus, we hypothesize that the mesoscale shear of anticyclone catalyzed and enhanced the wave-driven mixing. The strong stratification may have additionally altered the characteristics of the propagating waves.

However, tidally-forced IW amplified by mesoscale shear in the CHL are not unique to the limited survey. Time series from the mooring show waves at approximately 2, 3 and 4 cpd associated with $\mathbf{u}'_{\uparrow}$ throughout the deployment (Figure 4c). A sheared background flow in the upper ocean, caused by spatial density gradients (thermal wind), a meandering boundary current, or eddies, could therefore enhance IW-derived shear. An analysis of kinetic energy associated with upward-propagating IW, $\mathrm{HKE}_{\uparrow}$, variance of upward propagating IW shear $\mathbf{S}_{\uparrow}$, and the amplitude of mesoscale shear, $|\mathbf{S}_{\mathrm{meso}}|$, substantiates this claim. Using all observations in the upper 300 m and in 3-day moving windows, the variance of $\mathbf{S}_{\uparrow}$, binned in average $\mathrm{HKE}_{\uparrow}$ and $|\mathbf{S}_{\mathrm{meso}}|$ shows a pattern: the shear variance increases with both increasing $\mathrm{HKE}_{\uparrow}$ and $|\mathbf{S}_{\mathrm{meso}}|$ (Figure 4d). That is, when energetic upward propagating waves and mesoscale shear coexist, the IW shear variance is amplified.

This conceptually simplified analysis does not capture the full complexity of interactions of internal waves with mesoscale dynamics (e.g., Asselin et al., 2020; Rama et al., 2022; Thomas et al., 2020; Whalen et al., 2018). We further note that near-inertial internal tides are likely affected differently than the higher compound/harmonic frequencies, as these are less susceptible to blocking by relative vorticity. Overall, the mooring-based analysis supports dynamical interactions between the shear from internal waves generated by tidal flow over topography and the eddying background current in northern Fram Strait, posing an energy source for upper ocean turbulence.

4. Discussion

Near-inertial and superinertial IW can also be emitted from spontaneous generation through the loss of balance of fronts or eddies (Chouksey et al., 2022; Shakespeare & Hogg, 2018), from trapped waves in anticyclones (e.g., Kunze, 1985; Thomas et al., 2024), or as radial waves (e.g., Johannessen et al., 2019). These alternative explanations for the IW near the eddy would have intriguing implications, with eddies acting as mobile sources of wave-driven mixing in the ice-covered upper ocean. However, as the frequency content of the oscillating shear, with dominant clockwise $\sim$3 cpd, matches spectral peaks in the mooring data, and similar superinertial peaks from nonlinear interactions have been reported in the region before, both from observations (Fer et al., 2010; Padman & Dillon, 1991) and model simulations (Urbancic et al., 2022; Wang et al., 2022), we argue that this implies tidal forcing as the most likely generation mechanism for these IW.

Halocline mixing drives variability in the marine ecosystem. The distinct layering of chlorophyll-a and oxygen supersaturation is symptomatic of a balance between nutrient and light availability, reinforced by suppressed vertical transport (e.g., Cherkasheva et al., 2014; von Appen et al., 2021). Turbulence affects the plankton growth rate through vertical displacements into depths with increased or decreased light availability, and through turbulent resupply of nutrients. Stratification may limit primary production if the nutrient supply halts. Wind-driven mixing events can erode the seasonal halocline and enable late plankton blooms in fall by mixing nutrients upward (Ardyna et al., 2014; Castro de la Guardia et al., 2019). As opposed to such episodic replenishment, we suggest that regions with mixing caused by upward-propagating internal waves experience a more gradual nutrient resupply, potentially extending summer blooms.

Northern Fram Strait is dynamically distinct in several ways: (a) the Rossby radius is small ($3 - 8$ km; Nurser & Bacon, 2014; von Appen et al., 2016), much smaller than in lower latitudes, and smaller than horizontal scales of low-mode internal tides, (b) there are strong cross-slope tidal currents, (c) the seasonal meltwater stratification allows IW to propagate into the boundary layer, and (d) semidiurnal tides are near-inertial. That is, small changes in vorticity can allow or block internal tide propagation before waves reach the surface ocean.

Despite these regional specifics, our findings may be applicable to other areas. Along the shelf break of the Arctic Ocean's margins, the flow over rough topography excites tidally-forced lee waves (Fer et al., 2022; Rippeth et al., 2015), mixing heat of the Atlantic Water layer upward. These regions also exhibit enhanced eddy kinetic energy (EKE; von Appen et al., 2022), as eddies peel off the boundary current. We also expect the interaction of mesoscale shear with internal tides (and overtones/compound frequencies) to enhance mixing in the upper ocean there.

The projected increase of EKE in the Arctic Ocean (Li et al., 2024) and the more seasonal ice cover may lead to increased relevance of mesoscale dynamics interacting with tidally-forced waves. This may partly counteract the suggested decrease of near-surface dissipation of EKE when sea ice declines (Manucharyan & Thompson, 2022). A quantification of the involved energetics, from tidal conversion, via mesoscale-wave interactions, down to dissipation, would be desirable.

The environmental conditions of Weddell Sea in the Southern Ocean are also comparable to Fram Strait; a small Rossby radius (<10 km; Chelton et al., 1998), meltwater-derived surface stratification in summer (e.g., Flynn et al., 2021), and energetic, near-inertial tides with spectral peaks at superinertial frequencies (see Pinner et al. (2025), their Figure 3; and Daae et al. (2009), their Figure 14). There, mixing through the interaction of superinertial waves with mesoscale variability could impact marine carbonate chemistry (Droste et al., 2022).

5. Conclusions and Implications

Fram Strait is characterized by energetic eddies, strong tidal currents interacting with topography, and pronounced near-surface stratification from meltwater in summer. In this regime, we have presented detailed observations showing upward-propagating waves actively driving turbulence in the halocline above an anticyclone. Using mooring observations, we have demonstrated that these waves were generated by tidal forcing at the seafloor, and amplified by the mesoscale shear near the surface. Particularly the observed impact of higher-frequency waves, energized by nonlinear wave-wave interactions, offers novel insights into the energy pathways from tidal conversion at the seafloor to turbulent mixing in the upper Arctic Ocean. This process may also occur in areas along the shelf break in the Arctic Ocean where energetic tides are present.

The seasonal halocline is typically considered a barrier to turbulent transport, limiting deep-reaching mixing from the already weak atmospheric forcing in summer. We suggest that bottom-generated internal waves can then become relatively important for driving near-surface mixing. Thus, the seasonal halocline is not just a barrier, it also provides a pathway for wave propagation and wave-driven turbulence.

Potential consequences of these dynamics include prolonged plankton blooms, which impact the ecosystem, and–speculatively–enhanced heat entrainment into the convective mixed layer in winter, likely slowing down ice growth. As the internal waves may draw energy from the mesoscale flow before dissipating, another effect of the observed dynamics is the modification of near-surface, cross-scale kinetic energy transfers.

Therefore, we argue that it is crucial to quantify the role of tidally forced waves and their interaction with mesoscale features on upper ocean mixing in the Arctic. This could be achieved through mooring arrays capable of resolving both internal tide energy flux divergence and mesoscale dynamics, in combination with turbulence-resolving instrumentation. Other relevant aspects include the interaction of rotating wave shear with the sheared flow from surface stress, and the role of nonlinear internal tides. Moorings or floats with biogeochemical profiling capabilities could provide insights into subsequent nutrient transport. These efforts may be complemented with modeling studies to disentangle the relative effect of wave-driven mixing in the upper ocean compared to other forcings. Together, these approaches will advance our understanding of Arctic Ocean mixing processes and their effects on sea ice and the ecosystem.

Data Availability Statement

The microstructure observations, the 300 kHz ADCP measurements, and the mooring data are available from Reifenberg, Fer, et al. (2025a); Fer and Reifenberg (2025b); Fer et al. (2025), respectively. The vessel-mounted ADCP data are available from Reifenberg, Hofmann, et al. (2025).

Geophysical Research Letters 10.1029/2025GL117468

Acknowledgments
The fieldwork was supported by Grants AWI_PS131_07 and AWI_PS137_09. The authors thank everyone on RV Polarstern for their support in the field, especially Fiona Elliott, Zerlina Hofmann, Mario Hoppmann, Laura Mathieu, and Rebecca McPherson for supporting the MSS sampling on the ice. SR received funding from the Helmholtz Graduate School for Polar and Marine Research (POLMAR) for a research stay in Bergen, Norway. IF received funding from the Office of Naval Research–Global, Grant/award number N62909-22-1-2023. The authors kindly thank Wilken-Jon von Appen and Torsten Kanzow for valuable discussions throughout the entire evolution of this study. Open Access funding enabled and organized by Projekt DEAL.

References

Ardyna, M., & Arrigo, K. R. (2020). Phytoplankton dynamics in a changing Arctic Ocean. *Nature Climate Change*, *10*(10), 892–903. https://doi.org/10.1038/s41558-020-0905-y

Ardyna, M., Babin, M., Gosselin, M., Devred, E., Rainville, L., & Tremblay, J.-É. (2014). Recent Arctic Ocean sea ice loss triggers novel fall phytoplankton blooms. *Geophysical Research Letters*, *41*(17), 6207–6212. https://doi.org/10.1002/2014GL061047

Artana, C., Provost, C., Ferrari, R., Bricaud, C., Poli, L., & Park, Y.-H. (2022). Tides, internal and near-inertial waves in the Yermak pass at the entrance of the Atlantic water to the Arctic Ocean. *Journal of Geophysical Research: Oceans*, *127*(12), e2022JC019082. https://doi.org/10.1029/2022JC019082

Asselin, O., Thomas, L. N., Young, W. R., & Rainville, L. (2020). Refraction and straining of near-inertial waves by barotropic eddies. *Journal of Physical Oceanography*, *50*(12), 3439–3454. https://doi.org/10.1175/JPO-D-20-0109.1

Athanase, M., Provost, C., Artana, C., Pérez-Hernández, M. D., Sennéchael, N., Bertosio, C., et al. (2021). Changes in Atlantic water circulation patterns and volume transports north of Svalbard over the last 12 Years (2008–2020). *Journal of Geophysical Research: Oceans*, *126*(1). https://doi.org/10.1029/2020JC016825

Baumann, T. M., & Fer, I. (2023). Trapped tidal currents generate freely propagating internal waves at the Arctic continental slope. *Scientific Reports*, *13*(1), 14816. https://doi.org/10.1038/s41598-023-41870-3

Carmack, E., Polyakov, I., Padman, L., Fer, I., Hunke, E., Hutchings, J., et al. (2015). Toward quantifying the increasing role of oceanic heat in sea ice loss in the new arctic. *Bulletin of the American Meteorological Society*, *96*(12), 2079–2105. https://doi.org/10.1175/BAMS-D-13-00177.1

Castro de la Guardia, L., Garcia-Quintana, Y., Claret, M., Hu, X., Galbraith, E. D., & Myers, P. G. (2019). Assessing the role of high-frequency winds and sea ice loss on arctic phytoplankton blooms in an ice-ocean-biogeochemical model. *Journal of Geophysical Research: Biogeosciences*, *124*(9), 2728–2750. https://doi.org/10.1029/2018JG004869

Chelton, D. B., deSzoeke, R. A., Schlax, M. G., El Naggar, K., & Siwertz, N. (1998). Geographical variability of the first baroclinic Rossby radius of deformation. *Journal of Physical Oceanography*, *28*(3), 433–460. https://doi.org/10.1175/1520-0485(1998)028<0433:GVOTFB>2.0.CO;2

Cherkasheva, A., Bracher, A., Melsheimer, C., Köberle, C., Gerdes, R., Nöthig, E.-M., et al. (2014). Influence of the physical environment on polar phytoplankton blooms: A case study in the Fram Strait. *Journal of Marine Systems*, *132*, 196–207. https://doi.org/10.1016/j.jmarsys.2013.11.008

Chouksey, M., Eden, C., & Olbers, D. (2022). Gravity wave generation in balanced sheared flow revisited. *Journal of Physical Oceanography*, *52*(7), 1351–1362. https://doi.org/10.1175/JPO-D-21-0115.1

Daae, K. L., Fer, I., & Abrahamsen, E. P. (2009). Mixing on the continental slope of the southern weddell sea. *Journal of Geophysical Research*, *114*(C9). https://doi.org/10.1029/2008JC005259

Droste, E. S., Hoppema, M., González-Dávila, M., Santana-Casiano, J. M., Queste, B. Y., Dall'Olmo, G., et al. (2022). The influence of tides on the marine carbonate chemistry of a coastal polynya in the south-eastern Weddell Sea. *Ocean Science*, *18*(5), 1293–1320. https://doi.org/10.5194/os-18-1293-2022

Fer, I. (2014). Near-inertial mixing in the central Arctic Ocean. *Journal of Physical Oceanography*, *44*(8), 2031–2049. https://doi.org/10.1175/JPO-D-13-0133.1

Fer, I., Baumann, T. M., Koenig, Z., Muilwijk, M., & Tippenhauer, S. (2022). Upper-Ocean turbulence structure and ocean-ice drag coefficient estimates using an ascending microstructure profiler during the MOSAiC drift. *Journal of Geophysical Research: Oceans*, *127*(9), e2022JC018751. https://doi.org/10.1029/2022JC018751

Fer, I., Dengler, M., Holtermann, P., Le Boyer, A., & Lueck, R. (2024). ATOMIX benchmark datasets for dissipation rate measurements using shear probes. *Scientific Data*, *11*(1), 518. https://doi.org/10.1038/s41597-024-03323-y

Fer, I., Elliott, F., Hoppmann, M., Kanzow, T., Reifenberg, S. F., & von Appen, W.-J. (2025). Ocean current, temperature and salinity measurements from a mooring at the Yermak Plateau, July 2022–July 2023 [dataset]. *Norwegian Marine Data Centre*. https://doi.org/10.21335/NMDC-550637823

Fer, I., Koenig, Z., Kozlov, I. E., Ostrowski, M., Rippeth, T. P., Padman, L., et al. (2020). Tidally forced lee waves drive turbulent mixing along the Arctic Ocean margins. *Geophysical Research Letters*, *47*(16), e2020GL088083. https://doi.org/10.1029/2020GL088083

Fer, I., Müller, M., & Peterson, A. K. (2015). Tidal forcing, energetics, and mixing near the Yermak Plateau. *Ocean Science*, *11*(2), 287–304. https://doi.org/10.5194/os-11-287-2015

Fer, I., Peterson, A. K., & Nilsen, F. (2023). Atlantic water boundary current along the southern Yermak Plateau, Arctic Ocean. *Journal of Geophysical Research: Oceans*, *128*(6), e2023JC019645. https://doi.org/10.1029/2023JC019645

Fer, I., & Reifenberg, S. F. (2025a). Dissipation measurements using an MSS profiler in summer 2022, during the RV Polarstern PS131 cruise, ATWAICE [dataset]. *PANGAEA*. https://doi.org/10.1594/PANGAEA.977637

Fer, I., & Reifenberg, S. F. (2025b). Ocean velocity profiles under drifting ice floes measured by an ice-mounted 300 kHz ADCP northwest of Svalbard during RV POLARSTERN cruise PS131 (ATWAICE), July–August 2022 [dataset]. *PANGAEA*. https://doi.org/10.1594/PANGAEA.978165

Fer, I., Skogseth, R., & Geyer, F. (2010). Internal waves and mixing in the marginal ice zone near the Yermak Plateau. *Journal of Physical Oceanography*, *40*(7), 1613–1630. https://doi.org/10.1175/2010JPO4371.1

Fer, I., & Sundfjord, A. (2007). Observations of upper ocean boundary layer dynamics in the marginal ice zone. *Journal of Geophysical Research*, *112*(C4), C04012. https://doi.org/10.1029/2005JC003428

Flynn, R. F., Bornman, T. G., Burger, J. M., Smith, S., Spence, K. A. M., & Fawcett, S. E. (2021). Summertime productivity and carbon export potential in the Weddell Sea, with a focus on the waters adjacent to Larsen C Ice Shelf. *Biogeosciences*, *18*(22), 6031–6059. https://doi.org/10.5194/bg-18-6031-2021

Hattermann, T., Isachsen, P. E., von Appen, W.-J., Albretsen, J., & Sundfjord, A. (2016). Eddy-driven recirculation of Atlantic water in Fram Strait. *Geophysical Research Letters*, *43*(7), 3406–3414. https://doi.org/10.1002/2016GL068323

He, Y., & Lamb, K. G. (2022). Effects of an along-shelf current on the generation of internal tides near the critical latitude. *Journal of Fluid Mechanics*, *932*, A55. https://doi.org/10.1017/jfm.2021.1071

Hersbach, H., Bell, B., Berrisford, P., Biavati, G., Horányi, A., Muñoz Sabater, J., et al. (2023). ERA5 hourly data on single levels from 1940 to present. *Copernicus Climate Change Service (C3S) Climate Data Store (CDS)*. https://doi.org/10.24381/cds.adbb2d47

Hofmann, Z., von Appen, W.-J., & Wekerle, C. (2021). Seasonal and mesoscale variability of the two Atlantic water recirculation pathways in Fram Strait. *Journal of Geophysical Research: Oceans*, *126*(7), e2020JC017057. https://doi.org/10.1029/2020JC017057

Ivanov, V., Alexeev, V., Koldunov, N. V., Repina, I., Sandø, A. B., Smedsrud, L. H., & Smirnov, A. (2016). Arctic Ocean heat impact on regional ice decay: A suggested positive feedback. *Journal of Physical Oceanography*, *46*(5), 1437–1456. https://doi.org/10.1175/JPO-D-15-0144.1

Johannessen, O. M., Sandven, S., Chunchuzov, I. P., & Shuchman, R. A. (2019). Observations of internal waves generated by an anticyclonic eddy: A case study in the ice edge region of the Greenland sea. *Tellus A: Dynamic Meteorology and Oceanography*, *71*(1), 1652881. https://doi.org/10.1080/16000870.2019.1652881

Kunze, E. (1985). Near-inertial wave propagation in geostrophic shear. *Journal of Physical Oceanography*, *15*(5), 544–565. https://doi.org/10.1175/1520-0485(1985)015<0544:NIWPIG>2.0.CO;2

Leaman, K. D., & Sanford, T. B. (1975). Vertical energy propagation of inertial waves: A vector spectral analysis of velocity profiles. *Journal of Geophysical Research (1896–1977)*, *80*(15), 1975–1978. https://doi.org/10.1029/JC080i015p01975

Lester, C. W., Wagner, T. J. W., McNamara, D. E., & Cape, M. R. (2021). The influence of meltwater on phytoplankton blooms near the sea-ice edge. *Geophysical Research Letters*, *48*(2), e2020GL091758. https://doi.org/10.1029/2020GL091758

Li, X., Wang, Q., Danilov, S., Koldunov, N., Liu, C., Müller, V., et al. (2024). Eddy activity in the Arctic Ocean projected to surge in a warming world. *Nature Climate Change*, *14*(2), 156–162. https://doi.org/10.1038/s41558-023-01908-w

Lueck, R., Fer, I., Bluteau, C., Dengler, M., Holtermann, P., Inoue, R., et al. (2024). Best practices recommendations for estimating dissipation rates from shear probes. *Frontiers in Marine Science*, *11*. https://doi.org/10.3389/fmars.2024.1334327

Manley, T. O. (1995). Branching of atlantic water within the Greenland-spitsbergen passage: An estimate of recirculation. *Journal of Geophysical Research*, *100*(C10), 20627–20634. https://doi.org/10.1029/95JC01251

Manucharyan, G. E., & Thompson, A. F. (2017). Submesoscale Sea ice-ocean interactions in marginal ice zones. *Journal of Geophysical Research: Oceans*, *122*(12), 9455–9475. https://doi.org/10.1002/2017JC012895

Manucharyan, G. E., & Thompson, A. F. (2022). Heavy footprints of upper-ocean eddies on weakened Arctic sea ice in marginal ice zones. *Nature Communications*, *13*(1), 2147. https://doi.org/10.1038/s41467-022-29663-0

Martin, T., Tsamados, M., Schroeder, D., & Feltham, D. L. (2016). The impact of variable sea ice roughness on changes in Actic ocean surface stress: A model study. *Journal of Geophysical Research: Oceans*, *121*(3), 1931–1952. https://doi.org/10.1002/2015JC011186

McDougall, T. J., & Barker, P. M. (2011). *Getting started with TEOS-10 and the gibbs seawater (GSW) oceanographic toolbox*. SCOR/IAPSO WG127.

McPherson, R., Wekerle, C., & Kanzow, T. (2023). Shifts of the recirculation pathways in central Fram Strait drive Atlantic intermediate water variability on northeast Greenland shelf. *Journal of Geophysical Research: Oceans*, *128*(10), e2023JC019915. https://doi.org/10.1029/2023JC019915

Murray, A., Ramondenc, S., Reifenberg, S. F., Jucker, M., Neudert, M., McPherson, R., et al. (2025). Eukaryotic biodiversity of sub-ice water in the marginal ice zone of the European arctic: A multi-marker eDNA metabarcoding survey. *Science of the Total Environment*, *968*, 178840. https://doi.org/10.1016/j.scitotenv.2025.178840

Nurser, A. J. G., & Bacon, S. (2014). The Rossby radius in the Arctic Ocean. *Ocean Science*, *10*(6), 967–975. https://doi.org/10.5194/os-10-967-2014

Padman, L., & Dillon, T. M. (1991). Turbulent mixing near the Yermak Plateau during the coordinated eastern arctic experiment. *Journal of Geophysical Research*, *96*(C3), 4769–4782. https://doi.org/10.1029/90JC02260

Padman, L., Plueddemann, A. J., Muench, R. D., & Pinkel, R. (1992). Diurnal tides near the Yermak Plateau. *Journal of Geophysical Research*, *97*(C8), 12639–12652. https://doi.org/10.1029/92JC01097

Pinner, O., Pollmann, F., Janout, M., Voet, G., & Kanzow, T. (2025). Internal-wave-induced dissipation rates in the Weddell Sea bottom water gravity current. *Ocean Science*, *21*(2), 701–726. https://doi.org/10.5194/os-21-701-2025

Polyakov, I. V., Pnyushkov, A. V., Charette, M., Cho, K.-H., Jung, J., Kipp, L., et al. (2025). Atlantification advances into the Amerasian basin of the Arctic Ocean. *Science Advances*, *11*(8), eadq7580. https://doi.org/10.1126/sciadv.adq7580

Rama, J., Shakespeare, C. J., & Hogg, A. M. (2022). Importance of background vorticity effect and Doppler shift in defining near-inertial internal waves. *Geophysical Research Letters*, *49*(22), e2022GL099498. https://doi.org/10.1029/2022GL099498

Randelhoff, A., Fer, I., & Sundfjord, A. (2017). Turbulent upper-Ocean Mixing affected by meltwater layers during arctic summer. *Journal of Physical Oceanography*, *47*(4), 835–853. https://doi.org/10.1175/JPO-D-16-0200.1

Reifenberg, S. F., Fer, I., Kanzow, T., von Appen, W.-J., Hoppmann, M., Krumpen, T., et al. (2025a). Turbulence observations below drifting sea ice: TKE production and dissipation in the meltwater-influenced boundary layer. *Journal of Physical Oceanography*, *55*(4), 451–470. https://doi.org/10.1175/JPO-D-24-0102.1

Reifenberg, S. F., Hofmann, Z., von Appen, W.-J., & Kanzow, T. (2025b). Ocean velocity data from a vessel-mounted acoustic Doppler current profiler from a day-long ice-drift station during the PS131 expedition with RV Polarstern in July 2022 [dataset]. *Zenodo*. https://doi.org/10.5281/zenodo.15525269

Rippeth, T., & Fine, E. (2022). Turbulent mixing in a changing Arctic Ocean. *Oceanography*. https://doi.org/10.5670/oceanog.2022.103

Rippeth, T., Lincoln, B. J., Lenn, Y.-D., Green, J. A. M., Sundfjord, A., & Bacon, S. (2015). Tide-mediated warming of Arctic halocline by Atlantic heat fluxes over rough topography. *Nature Geoscience*, *8*(3), 191–194. https://doi.org/10.1038/ngeo2350

Rippeth, T., Vlasenko, V., Stashchuk, N., Scannell, B. D., Green, J. A. M., Lincoln, B. J., & Bacon, S. (2017). Tidal conversion and mixing poleward of the critical latitude (an arctic case study). *Geophysical Research Letters*, *44*(24). https://doi.org/10.1002/2017GL075310

Schourup-Kristensen, V., Wekerle, C., Danilov, S., & Völker, C. (2021). Seasonality of mesoscale phytoplankton control in eastern Fram Strait. *Journal of Geophysical Research: Oceans*, *126*(10), e2021JC017279. https://doi.org/10.1029/2021JC017279

Shakespeare, C. J., & Hogg, A. M. (2018). The life cycle of spontaneously generated internal waves. *Journal of Physical Oceanography*, *48*(2), 343–359. https://doi.org/10.1175/JPO-D-17-0153.1

Silvester, J. M., Lenn, Y.-D., Polton, J. A., Rippeth, T. P., & Maqueda, M. M. (2014). Observations of a diapycnal shortcut to adiabatic upwelling of Antarctic circumpolar deep water. *Geophysical Research Letters*, *41*(22), 7950–7956. https://doi.org/10.1002/2014GL061538

Sumata, H., de Steur, L., Gerland, S., Divine, D., & Pavlova, O. (2021). Unprecedented decline of Arctic sea ice outflow in 2018. *Nature Communications*, *13*(1), 1747. https://doi.org/10.1038/s41467-022-29470-7

Thomas, L. N., Moum, J. N., Qu, L., Hilditch, J. P., Kunze, E., Rainville, L., & Lee, C. M. (2024). Blocked drainpipes and smoking chimneys: Discovery of new near-inertial wave phenomena in anticyclones. *Oceanography*. https://doi.org/10.5670/oceanog.2024.304

Thomas, L. N., Rainville, L., Asselin, O., Young, W. R., Girton, J., Whalen, C. B., et al. (2020). Direct observations of near-inertial wave - refraction in a dipole vortex. *Geophysical Research Letters*, *47*(21), e2020GL090375. https://doi.org/10.1029/2020GL090375

Urbancic, G. H., Lamb, K. G., Fer, I., & Padman, L. (2022). The generation of linear and nonlinear internal waves forced by subinertial tides over the Yermak Plateau, Arctic Ocean. *Journal of Physical Oceanography*, *52*(9), 2183–2203. https://doi.org/10.1175/JPO-D-21-0264.1

Voet, G., Waterhouse, A. F., Savage, A., Kunze, E., MacKinnon, J. A., Alford, M., et al. (2024). Near-inertial energy variability in a strong mesoscale eddy field in the Iceland basin. *Oceanography*, *37*(4), 34–47. https://doi.org/10.5670/oceanog.2024.302

von Appen, W.-J., Baumann, T. M., Janout, M., Koldunov, N., Lenn, Y.-D., Pickart, R., et al. (2022). Eddies and the distribution of eddy kinetic energy in the Arctic Ocean. *Oceanography*, *35*(3–4), 42–51. https://doi.org/10.5670/oceanog.2022.122

von Appen, W.-J., Schauer, U., Hattermann, T., & Beszczynska-Möller, A. (2016). Seasonal cycle of mesoscale instability of the West spitsbergen current. *Journal of Physical Oceanography*, *46*(4), 1231–1254. https://doi.org/10.1175/JPO-D-15-0184.1

von Appen, W.-J., Waite, A. M., Bergmann, M., Bienhold, C., Boebel, O., Bracher, A., et al. (2021). Sea-ice derived meltwater stratification slows the biological carbon pump: Results from continuous observations. *Nature Communications*, *12*(1), 7309. https://doi.org/10.1038/s41467-021-26943-z

Wang, S., Cao, A., Li, Q., & Chen, X. (2022). Diurnal and semidiurnal internal waves on the southern slope of the Yermak Plateau. *Scientific Reports*, *12*(1), 11682. https://doi.org/10.1038/s41598-022-15662-0

Wekerle, C., Hattermann, T., Wang, Q., Crews, L., von Appen, W.-J., & Danilov, S. (2020). Properties and dynamics of mesoscale eddies in Fram Strait from a comparison between two high-resolution ocean–sea ice models. *Ocean Science*, *16*(5), 1225–1246. https://doi.org/10.5194/os-16-1225-2020

Whalen, C. B., MacKinnon, J. A., & Talley, L. D. (2018). Large-scale impacts of the mesoscale environment on mixing from wind-driven internal waves. *Nature Geoscience*, *11*(11), 842–847. https://doi.org/10.1038/s41561-018-0213-6

References From the Supporting Information

de Jong, M. F., Bower, A. S., & Furey, H. H. (2014). Two years of observations of warm-core anticyclones in the Labrador Sea and their seasonal cycle in heat and salt stratification. *Journal of Physical Oceanography*, *44*(2), 427–444. https://doi.org/10.1175/JPO-D-13-070.1

Gregg, M. C. (2021). *Ocean mixing* (1st ed.). Cambridge University Press. https://doi.org/10.1017/9781316795439

Ivey, G., Winters, K., & Koseff, J. (2008). Density stratification, turbulence, but how much mixing? *Annual Review of Fluid Mechanics*, *40*(40), 169–184. [Journal Article]. https://doi.org/10.1146/annurev.fluid.39.050905.110314

May, B. D., & Kelley, D. E. (2001). Growth and steady state stages of thermohaline intrusions in the Arctic Ocean. *Journal of Geophysical Research*, *106*(C8), 16783–16794. https://doi.org/10.1029/2000JC000605

Pawlowicz, R., Beardsley, B., & Lentz, S. (2002). Classical tidal harmonic analysis including error estimates in MATLAB using T_TIDE. *Computers and Geosciences*, *28*(8), 929–937. https://doi.org/10.1016/S0098-3004(02)00013-4

Ruddick, B. (1983). A practical indicator of the stability of the water column to double-diffusive activity. *Deep-Sea Research, Part A: Oceanographic Research Papers*, *30*(10), 1105–1107. https://doi.org/10.1016/0198-0149(83)90063-8